DUAL-POLARIZATION HAIL SIGNATURES ABOVE THE MELTING LAYER IN THUNDERSTORMS

Alexis Hunzinger[1], Kiel Ortega[2,3], and Jeffrey Snyder[2,3]

[1]National Weather Center Research Experiences for Undergraduates Program
Norman, Oklahoma
[2]Univ. of Oklahoma/Cooperative Institute for Mesoscale Meteorology Studies
Norman, Oklahoma
[3]NOAA/OAR/National Severe Storms Laboratory
Norman, Oklahoma

ABSTRACT

Identification and sizing of hail is important for warning operations and post-storm activities, such as identifying where the largest hail may have fallen. Recently the National Weather Service in the United States upgraded its operational radar fleet to polarimetric capabilities. Dual-polarization variables, such as differential reflectivity (Z_{DR}) and correlation coefficient (*CC*), can be useful in not only identifying areas with hail, but also the size of that hail. The Severe Hazards Analysis and Verification Experiment (SHAVE), run by CIMMS and the National Severe Storms Laboratory in Norman, OK, is tasked with collecting reports of hail, including maximum and average sizes, hail fall times, and ground coverage, in the wake of thunderstorms across the contiguous United States. The reports are collected at a high spatial resolution, with median report spacing near 2 km.

Eight cases with SHAVE reports were analyzed. These cases came from storms that were within 125 km of the nearest radar and produced at least 1 report of giant hail (diameter equal to or exceeding 51 mm). The primary signature investigated was the Z_{DR} column and attributes of those columns. The Z_{DR} column can be used as a proxy for updraft strength since it implies the lofting of supercooled liquid water droplets above the melting layer. These supercooled droplets may contribute to large hail growth. The Z_{DR} column height relative to the melting layer and the *CC* values within the Z_{DR} column were recorded. The location of the Z_{DR} column was compared to SHAVE reports. The goal for the analyses were to spatially and temporally relate the Z_{DR} column characteristics to the maximal surface hail size (e.g., does the appearance of a Z_{DR} column mean surface hail fall of a certain hail size within 20 minutes?). The results of the analyses and discussions on the feasibility of a Z_{DR} column algorithm and application of the results to the hail size discrimination algorithm will be presented.

1. INTRODUCTION

The detection of hail is important for the National Weather Service (NWS) when issuing warnings, especially when identifying storms that are considered severe. Currently the techniques for hail identification using single-polarization radar include the use of vertically integrated liquid (VIL; Greene and Clark 1972), VIL density (Amburn and Wolf 1997), the Hail Discrimination Algorithm (Witt et al. 1998a), reflectivity heights above environmental temperature heights (Donavon and Junbluth 2007), or the identification of three-body scatter spikes (Lemon 1998).

Corresponding author address: Alexis Hunzinger, National Weather Center Research Experiences for Undergraduates Program, Center for Analysis and Prediction of Storms, The University of Oklahoma, National Weather Center, 120 David L. Boren Blvd, Suite 2500, Norman, OK 73072
Email: a.e.hunzinger@gmail.com

When the NWS upgraded the WSR-88D to polarimetric capabilities in 2011, new radar products became available for operational use. These products include differential reflectivity (Z_{DR}) and correlation coefficient (*CC*). Z_{DR} is the logarithmic difference between the horizontal and vertical return power channels. An increasingly positive Z_{DR} identifies particles with increasingly horizontal orientations (i.e., large rain drops), while Z_{DR} values near 0 dB identify more spherical-shaped particles or tumbling particles, which may have no preferred orientation (i.e., large hailstones), and increasingly negative Z_{DR} values indicate increasingly vertical orientations (i.e., some types of ice crystals). *CC* is a measure of the correlation between the horizontal and vertical channels. A *CC* value of 1 indicates there is a strong correlation, with decreasing values showing lesser correlation. Values below 0.7 are typically considered non-meteorological. Depressed *CC* values may help indicate areas with mixed hydrometeors (i.e., rain and hail) or even the presence of giant hail (Balakrishnan and Zrnić 1990). Kumjian (2013a,b,c) outlines a description

of these new variables, their applications, and artifacts that present barriers to the proper analysis of these products.

Previous research for polarimetric hail detection is summarized in Heinselman and Ryzhkov (2006). A Hydrometeor Classification Algorithm (HCA; Park et al. 2009) has been implemented on the WSR-88D network and uses 6 polarimetric variables and variable derivatives to identify 10 hydrometeor classes with a fuzzy logic scheme. As implemented the HCA only identifies areas of rain and hail mix, not specific hail sizes. Ryzhkov et al. (2013a,b) used 1- and 2-D cloud modeling to develop an initial Hail Size Discrimination Algorithm (HSDA) which takes HCA designations, with a fuzzy logic scheme, of rain/hail and reclassifies those designations into 3 size classes: small (hailstone diameters less than 25 mm), large (hailstone diameters between 25 and 51 mm), and giant (hailstone diameters exceeding 51 mm). The importance of the HSDA is that hailstone melting is accounted for when determining the membership functions for the polarimetric variables for the 3 hail size classifications. This is compared to other hail detection techniques, such as Hail Differential Reflectivity (Aydin et al. 1986, Depue et al. 2007), which use the same relationship regardless of the melting state of hail. Ortega et al. (2015) evaluated the HSDA, along with developing observed, vertical profiles of polarimetric variables, and found the theoretical assumptions of Ryzhkov et al. (2013a) to be valid.

A limitation of the Ortega et al. (2015) study and the HSDA in general is that the updraft indicators above the melting level are not necessarily dependent on large values of horizontal reflectivity, Z_H. Above the melting level, the HSDA almost exclusively focuses upon high Z_H regions since Z_{DR} loses its discrimination power. The location of the updraft indicators may not be co-located with hail, but instead serve as a proxy to potential hail size produced by such an updraft. The weak echo, or bounded weak echo, region is one obvious signature (Warning Decistion Training Branch 2012). Another is the Z_{DR} column (Kumjian et al. 2012). This study will investigate the signatures above the melting level and try to better relate these signatures to surface hail fall.

2. BACKGROUND

2.1 Z_{DR} Columns

A thorough review plus a study into the anatomy, formation, and decay, of Z_{DR} columns can be found in Kumjian et al. (2014). The Z_{DR} column is a columnar shape of positive Z_{DR} values above the melting level. The Z_{DR} column is formed by the updraft lofting raindrops above the melting level. While larger raindrops may fall out of the updraft, smaller raindrops may be lofted to higher altitudes and colder temperatures. These drops may serve as hail embryos as they freeze during ascent. Since freezing is not instantaneous, the partially frozen drops could possibly be co-located with liquid water and completely frozen particles resulting in depressed *CC* values.

A result of the modeling within Kumjian et al. (2014) was the onset of increased hail mass at the surface following a peak in the Z_{DR} height. An observational study (Picca et al. 2011) found similar lags using Z_H area ratios (60-to-40 dBZ) below the melting level, instead of observed hail.

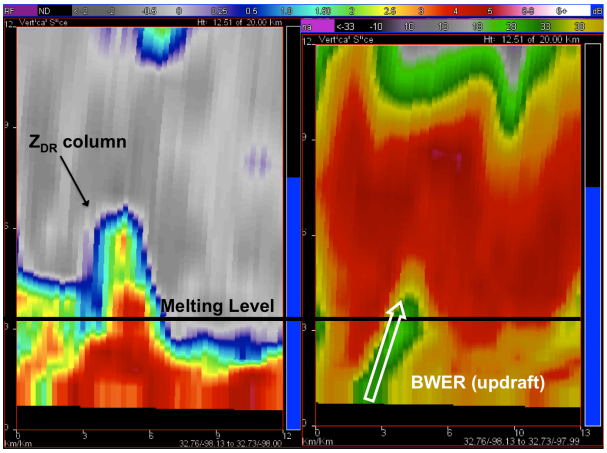

Figure 1: Cross-section of Z_{DR} (left) and Z_H (right). Note the co-location of the Z_{DR} column and BWER, confirming the location of the updraft.

2.2 *SHAVE*

The Severe Hazard Analysis and Verification Experiment (SHAVE), run by CIMMS and the National Severe Storms Laboratory in Norman, OK, is tasked with the collection of hail reports in the contiguous United States in the wake of thunderstorms (Ortega et al. 2009). Information on maximum and average sizes, hail fall times, and

ground coverage, is collected through phone surveys of impacted population. The reports are collected at a high spatial resolution, with a median spacing near 2 km (Fig. 2). The collection of null and non-severe reports is unique to SHAVE as this information would not normally appear in records of hail reports collected by the NWS and published within *Storm Data*. A limitation of the SHAVE reports is the time of the hail fall report is usually imprecise since SHAVE records the reports start and end time of hail fall in general, and not for the maximum hail size. However, SHAVE locations are generally accurate, which can allow for novel matching methods to pair SHAVE reports to storms.

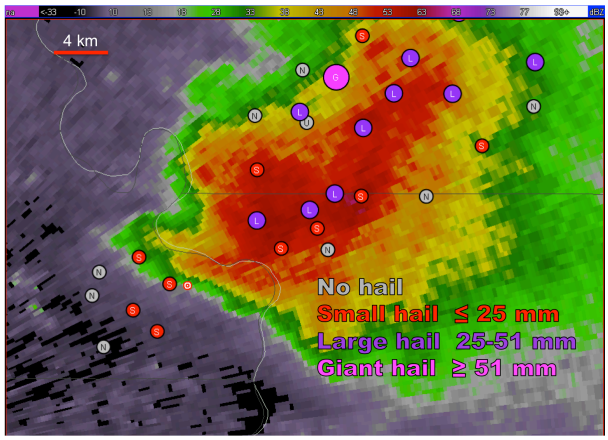

Figure 2: Plan view of Z_H with SHAVE reports from that storm. Spacing of reports can be inferred using legend for estimation. Hail category sizes listed. Hail considered severe when diameter exceeds 25 mm (1-in).

3. METHOD

3.1 *Cases*

Eight storms from a potential population of 26 were analyzed. The 18 cases excluded from this study were due to poor Z_{DR} calibrations, leading to false values of Z_{DR} column height. All storms were detected within 125 km of the nearest WSR-88D, produced at least one report of giant hail, and are classified as supercellular. All report data originated from SHAVE.

Date	Radar	No Hail	Small Hail	Large Hail	Giant Hail
15 May 2013	KFWS	7	7	25	19
21 June 2013	KABR	15	25	32	5
23 July 2013	KICT	7	6	12	19
21 May 2014	KILX	8	6	18	12
3 June 2014	KOAX	17	39	80	34
12 June 2014	KDYX	3	7	11	31
16 June 2014	KOAX	11	18	21	7
30 June 2014	KDMX	19	7	10	4

Figure 2: Table of cases analyzed.

3.2 *Products*

Polarimetric data from the nearest WSR-88D of the storm was first processed through the operational preprocessor (Istok et al. 2009). The preprocessor applies a number of corrections, including to Z_{DR} for system biases, and smooths the data along the radial. These smoothed fields are then used to generate the products used within this study. Four primary products were created for this study:

1) Z_{DR} column height, which was defined as the height of 0.5 dB above the height of the wet-bulb equal to 0ºC, $H(T_w=0ºC)$
2) *CC* at $H(T_w=0ºC)$ within the Z_{DR} column
3) *CC* at $H(T_w=-10ºC)$ within the Z_{DR} column
4) *CC* at $H(T_w=-20ºC)$ within the Z_{DR} column

Storms were manually interrogated to locate the Z_{DR} column and match the corresponding minimum isothermal *CC* values. Other attributes of the storm were also recorded, such as the presence of a three-body scatter spike or whether a weak-echo or bounded weak-echo region was present.

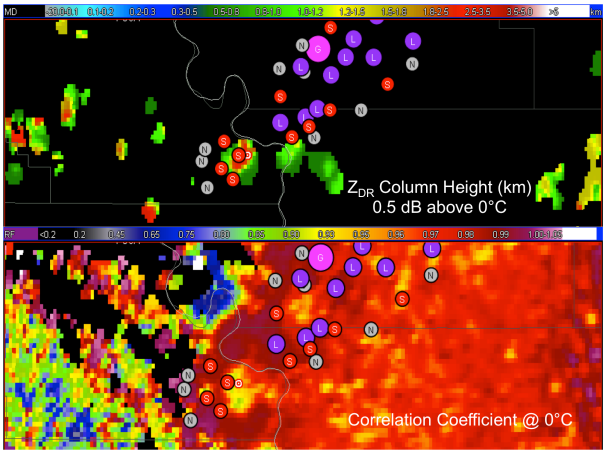

Figure 3: Plan view of Z_{DR} column height (top) and *CC* at 0ºC (bottom). Bullseye marker indicates same location. Note the depressed *CC* region associated with the Z_{DR} column.

3.3 *Storm Tracking and Lead Time*

The location of the Z_{DR} column was recorded along with the time of the 0.5 degree tilt of the corresponding volume. The locations and times of the Z_{DR} columns along a storm path were used to create a storm motion. This storm motion was used to pair the storm and the storm attributes with SHAVE reports that were downstream from the location.

Using longitude and latitude coordinates of the selected location, the storm motion was calculated between each time step. An initial 5 km half circle was then traced around the location of the Z_{DR} column with edges added to the half circle that deflected off the previously calculated storm motion by +/- 22.5 degrees. The polygon was "capped" at the locations downstream of the storm which were at a maximum of 35 minutes away from the storm location for the given storm motion. This polygon captures the track of the storm, as well as approximate lead times for hail fall. SHAVE reports were matched to the storm location using the storm motion and location and the report location. Figure 5 shows an estimation of lead times in one particular polygon.

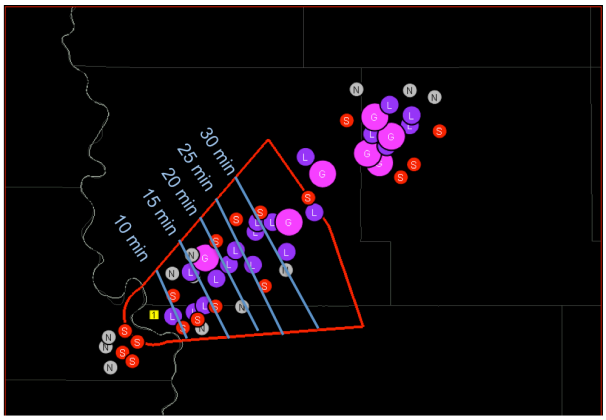

Figure 4: Example of polygon created using calculation of storm motion and lead time. Lead time lines approximated for visualization purposes.

4. RESULTS

4.1 Z_{DR} *Column Height*

In Figure 6, the evolution of Z_{DR} column height with time in a single storm shows several peaks in Z_{DR} column height. One peak is associated with the onset of large hail fall at the surface afterwards and another peak is associated with the onset of giant hail fall. Though these are peaks in Z_{DR} column height, they are not necessarily the absolute maximum. Additionally, not every local maximum is proceeded by large or giant hail. This general pattern was seen in each individual case.

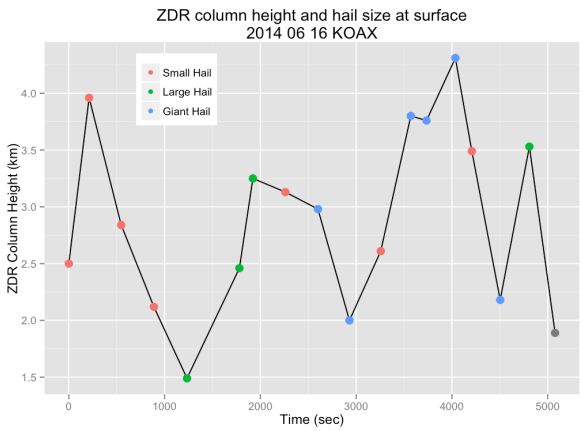

Figure 5: Evolution of Z_{DR} column height with time. Peaks in Z_{DR} column height preceding large hail fall and giant hail fall occur around 200 and 1900 seconds respectively.

In Figure 7, data from all cases was combined and the Z_{DR} column height and maximal hail fall were analyzed with respect to the lead time prior to observing hail at the surface. Results do not confirm a particular relationship. Surprisingly, the small hail during shorter lead times (0-5 min., <10min.) lean towards a higher Z_{DR} column height. However looking at large and giant hail, there appears to be no bias towards any particular height or lead time. The same plot was analyzed for each case individually with similar results.

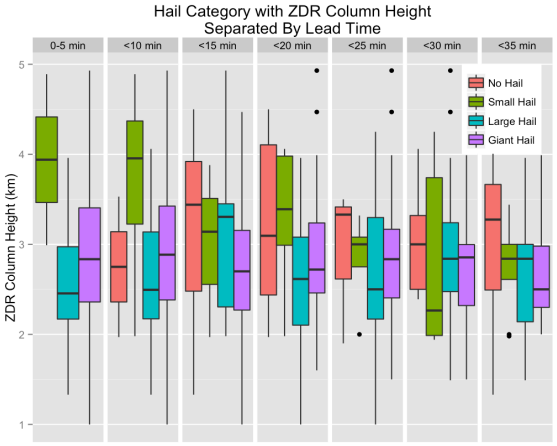

Figure 6: Hail categories associated with Z_{DR} column height separated by lead times.

4.2 *Minimum CC in Z_{DR} Column Height*

An analysis of the minimum *CC* within the Z_{DR} column at all isothermal levels revealed a qualitative "large" drop in *CC* at all levels prior to or just as giant hail was observed at the surface. No particular values or ranges were determined for the drop, though relative to the typical values for the storm, the drop appeared large. Additionally, the timing of the giant hail fall at the surface was not uniform among all cases, though the giant hail fall did occur after the drop in *CC*.

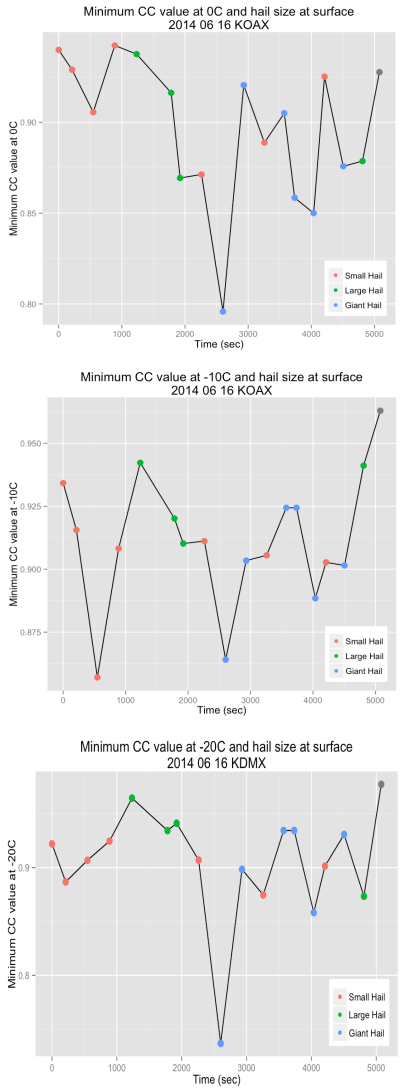

Figure 7: Minimum *CC* within the Z_{DR} column tracked for one case at three isothermal levels: 0ºC (top), -10ºC (middle), and -20ºC (bottom).

In an attempt to relate the minimum *CC* value within the Z_{DR} column at each isotherm to the height of the Z_{DR} column with respect to the category of hail at the surface, no real correlation appeared (Fig. 9). Each individual case was plotted in this manner and the same result was shown.

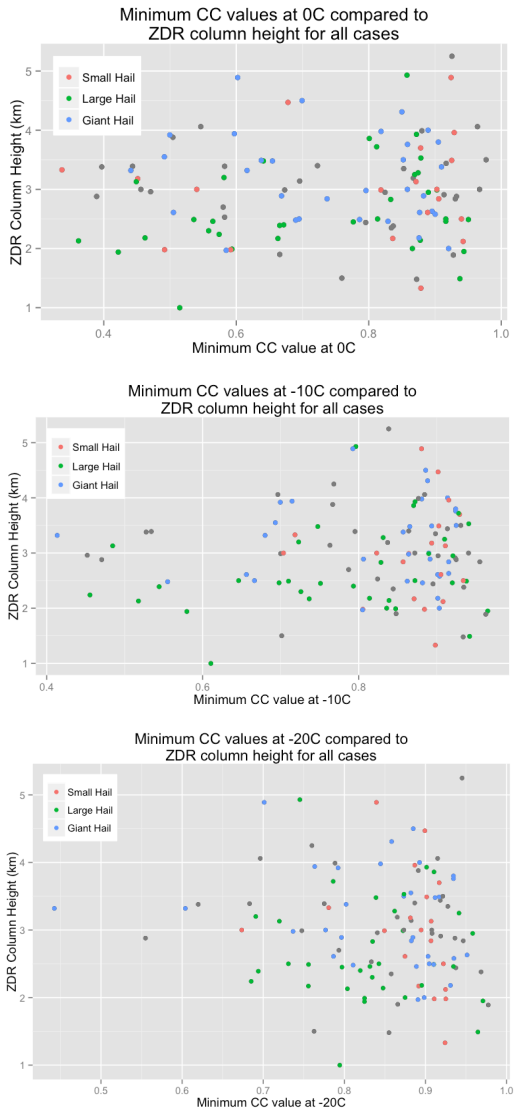

Figure 8: Z_{DR} column height compared to minimum *CC* within the Z_{DR} column by hail category. Minimum *CC* compared at three isothermal levels: 0ºC (top), -10ºC (middle), and -20ºC (bottom).

5. DISCUSSION

Proper Z_{DR} calibration is needed not just for proper manual interrogation of storms, but also for proper operation of algorithms, which rely on Z_{DR}. Many (~70%) of the available cases analyzed were excluded from analysis due to positive Z_{DR} bias. It is important that future operational support for the polarized WSR-88D fleet increase such that a random sample of events does not result in 70% of those cases resulting in poor research quality of polarimetric variables.

All of the thunderstorms analyzed were supercells and produced giant hail. These restrictions on the case types may have restricted the variety of results possible. It is possible that supercells share similarly structured Z_{DR} columns that do not behave the same or demonstrate the same results pertaining to giant hail fall that are expected. A greater variety of storm types and maximal hail sizes will be needed in the future to better understand the relationship between the Z_{DR} column and surface hail fall.

It is possible that the analysis was too narrow, focusing only on one primary feature, the Z_{DR} column, and its attributes. In order to fully analyze the evolution of Z_{DR} columns with respect to surface hail fall, investigating other features may be beneficial. For example, Picca and Ryzhkov (2012) indicate the value of analyzing high Z_H and the evolution and length of the three-body scatter spike in conjunction with other recognized features.

6. SUMMARY

Eight cases with SHAVE reports were analyzed. All eight cases were supercells that produced at least a single report of giant hail. The Z_{DR} column, and attributes thereof, were compared to maximal surface hail fall. No significant results were found. However, all cases analyzed displayed a decrease in minimum CC within the Z_{DR} column at 0ºC, -10ºC, and -20ºC, around the same time or just prior, giant hail fall was reported.

6. ACKNOWLEDGMENTS

This work was prepared by the authors with funding provided by National Science Foundation Grant No. AGS-1062932, and NOAA/Office of Oceanic and Atmospheric Research under NOAA-University of Oklahoma Cooperative Agreement #NA11OAR4320072, U.S. Department of Commerce. The statements, findings, conclusions, and recommendations are those of the author(s) and do not necessarily reflect the views of the National Science Foundation, NOAA, or the U.S. Department of Commerce.

7. REFERENCES

Amburn, S. A., and P. L. Wolf, 1997: VIL density as a hail indicator. *Wea. Forecasting*, **12**, 473-478.

Balakrishnan, N., and D.S. Zrnić, 1990: Estimation of rain and hail rates in mixed-phase precipitation. *J. Atmos. Sci.,* **47,** 565-583.

——, and ——, 1990a: Use of polarization to characterize precipitation and discriminate large hail. *J. Atmos. Sci.,* **47,** 1525-1540.

Blair, S. F., D. R. Deroche, J. M. Boustead, J. W. Leighton, B. L. Barjenbruch, and W. P. Gargan, 2011: A radar-based assessment of the detectability of giant hail. *Electronic J. Severe Storms Meteor.,* **6** (7), 1-30.

Conway, J. W., and D. S. Zrnić, 1993: A study of embryo production and hail growth using dual-Doppler and multiparameter radars. *Mon. Wea. Rev.*, **121,** 2511-2528.

Depue, T. K., P. C. Kennedy, and S. A. Rutledge, 2007: Performance of the hail differential reflectivity (H_{DR}) polarimetric radar hail indicator. *J. Appl. Meteor. Climatol.,* **46,** 1290-1301.

Donavon, R. A., and K. A. Jungbluth, 2007: Evaluation of a technique for radar identification of large hail across the Upper Midwest and Central Plains of the United States. *Wea. Forecasting,* **22,** 244-254.

Greene, D. R., and R. A. Clark, 1972: Vertically integrated liquid water —A new analysis tool. *Mon. Wea. Rev.,* **100,** 548-552.

Heinselman, P. L., and A. V. Ryzhkov, 2006: Validation of polarimetric hail detection. *Wea. Forecasting,* **21,** 839-850.

Hubbert, J., V. N. Bringi, L. D. Carey, and S. Bolen, 1998. CSU-CHILL polarimetric radar measurements from a severe hail storm in eastern Colorado. *J. Appl. Meteor.,* **37,** 749-775.

Istok, M. J., and Coauthors, 2009: WSR-88D dual polarization initial operating capabilities. *25th Conf. IIPS,* Amer. Meteor. Soc., Phoenix, AZ, 15.5. [Available online at https://ams.confex.com/ams/89annual/techprogram/paper_148927.htm].

Kumjian, M. R., 2013a: Principles and applications of dual-polarization weather radar. Part I: Description of the polarimetric radar variables. *J. Oper. Meteor.,* **1,** 226-242, doi:10.15191/nwajom.2013.0119.

——, 2013b: Principles and applications of dual-polarization weather radar. Part II: Warm and cold season applications. *J. Oper. Meteor.,* **1,** 243-264, doi:10.15191/nwajom.2013.0120.

——, 2013c: Principles and applications of dual-polarization weather radar. Part III: Artifacts. *J. Oper. Meteor.,* **1,** 265-274, doi:10.15191/nwajom.2013.0121.

——, and A. V. Ryzhkov, 2008: Polarimetric signatures in supercell thunderstorms. *J. Appl. Meteor. Climatol.,* **47,** 1940-1961, doi:10.1175/2007JAMC1874.1

——, S.M. Ganson, and A. V. Ryzhkov, 2012: Freezing of rain-drops in deep convective updrafts: A microphysical and polarimetric model. *J. Atmos. Sci.*, **69,** 3471-3490.

——, A. P. Khain, N. Benmoshe, E. Ilotoviz, A. V. Ryzhkov, and V. T. J. Phillips, 2014: The anatomy and physics of Z_{DR} column: Investigating a polarimetric radar signature with a spectral bin microphysical model. *J. Appl. Meteor. Climatol.,* **53,** 1820-1843, doi:10.1175/JAMC-D-13-0354.1

Lemon, L. R., 1998: The radar "three-body scatter spike": An operational large-hail signature. *Wea. Forecasting,* **13,** 327-340.

Ortega, K. L., T. M. Smith, K. L. Manross, A. G. Kolodziej, K. A. Scharfenberg, A. Witt, and J. J. Gourley, 2009: The Severe Hazard Analysis and Verification Experiment. *Bull. Amer. Meteor. Soc.,* **90,** 1519-1530.

——, J. M. Krause, and A. V. Ryzhkov, 2015: Polarimetric radar characteristics of melting hail: Part III: Validation of the algorithm for hail size discrimination. *J. Appl. Meteor. Climatol.,* in review

Park, H. S., A. V. Ryzhkov, D. S. Zrnić, and K. E. Kim, 2009: The hydrometeor classification for the polarimetric WSR-88D: Description and application to an MCS. *Wea. Forecasting*, **24,** 730-748.

Picca, J. C. and A. V. Ryzhkov, 2011: A dual-wavelength polarimetric analysis of the 16 May 2010 Oklahoma City extreme hailstorm. *Mon. Wea. Rev.,* **140,** 1385-1403, doi:10.1175/MWR-D-11-00112.1

Ryzhkov, A. V., M. R. Kumjian, S. M. Ganson, and P. Zhang, 2013a: Polarimetric radar characteristics of melting hail. Part I: Theoretical simulations using spectral microphysical modeling. *J. Appl. Meteor. Climatol.*, **52,** 2849-2870, doi:10.1175/JAMC-D-13-074.1

——, ——, ——, and P. Zhang, 2013b: Polarimetric radar characteristics of melting hail. Part II: Practical implications. *J. Appl.*

Meteor. Climatol., **52,** 2871-2886, doi:10.1175/JAMC-D-13-074.1

Warning Decision Training Branch cited 2012: WSR-88D distane learning operations course, Topic 7: Convective storm structure and evolution Lesson 6: Severe hail identification. [Available online at http://www.wdtb.noaa.gov/courses/dloc/outline.php].

Witt, A., M. D. Eilts, G. J. Strumpf, J. T. Johnson, E. D. Mitchell, and K. W. Thomas, 1998a: A enhanced hail detection algorithm for the WSR-88D. *Wea. Forecasting*, **13,** 286-303.